Molecular Catalysis 475 (2019) 110410

Contents lists available at ScienceDirect

Molecular Catalysis

journal homepage: www.elsevier.com/locate/mcat

Acylation of anisole with carboxylic acids catalyzed by tungsten oxide supported on titanium dioxide

Kazu Okumura*, Masaki Iida, Hajime Yamashita

Department of Applied Chemistry, School of Advanced Engineering, Kogakuin University, 2665-1 Nakano-machi Hachioji-city, 192-0015, Tokyo, Japan

ARTICLE INFO

Keywords:
Friedel-crafts acylation
Octanoic acid
Tungsten oxide
Titanium dioxide

ABSTRACT

Friedel-Crafts (F-C) acylation of anisole with octanoic acid was carried out on tungsten oxide (WO_3) supported on various types of oxide supports. We have found that the highest activity was obtained when TiO_2 was used as the support. WO_3/TiO_2 was found to be active in the acylation of anisole with carboxylic acids of varying alkyl chain lengths (C6–C10). It was possible to recycle the WO_3/TiO_2 catalyst for up to 5 times without deactivation. The turnover frequency (TOF) of the catalyst was closely correlated with the electronegativity of the cation of the support used for WO_3. When a strong basic oxide such as CeO_2 was used as a support, the acid strength of WO_3 was diminished, while the strong acidity of WO_3 was retained on a weak basic support like TiO_2. This explains why the acid strength and consequently, the activity, were found to be the highest for the WO_3/TiO_2 catalyst. The trend of the catalytic performance was consistent with the order of acid strength of WO_3 on different supports measured by temperature-programmed desorption of NH_3.

1. Introduction

Tungsten oxide (WO_3) has been used as a photocatalyst, gas sensor, and acid catalyst over the past several decades [1]. WO_3-based catalysts having acidic properties can be classified into several groups. One group includes WO_3 crystals and those doped with foreign elements in a nanowire structure, which are used as catalysts and gas sensors [2]. We have previously reported that WO_3 doped with Nb, prepared by co-precipitation and hydrothermal methods, is active in the Friedel-Crafts (F−C) reaction [3,4]. Another group of WO_3-based catalysts, i.e. overlayer structures or clusters of WO_3 supported on high-surface-area oxides have been found to be useful as photocatalysts [5], catalysts for alkene isomerization [6], dehydration of alcohols [7], and glucose dehydration to 5-hydroxymethylfurfural [8]. In the domain of WO_3-supported catalysts, it is widely accepted that acid properties emerge by the coating of the metal oxides on basic oxide supports [9]. However, the genesis of the catalytic activity of supported WO_3 is not still completely understood. Wachs et al. reported that WO_x clusters supported on the surface showed activity for partial oxidation of methanol [10]. Iglesia et al. suggested that proton evolution occurred in the WO_x upper layer on ZrO_2 in a manner similar to heteropolyanion formation [11]. Tanaka et al. proposed that a Brønsted acid site is generated at the boundary between the WO_3 upper layer domains [12]. Previous research was focused mainly on WO_x supported on specific supports. However, new insight into the origin of catalytic activity should be obtained by systematically correlating the catalytic performance and the acidic property of WO_3 loaded on different kinds of supports. For this purpose, four types of supports—CeO_2, ZrO_2, Al_2O_3 and TiO_2—were used in this study. F−C acylation using a carboxylic acid was carried out as the catalytic reaction over WO_3-loaded catalysts. F−C alkylation and acylation have been extensively studied using acid anhydrides and acid chlorides as acylating agents [13]. The use of these reagents result in the formation of carboxylic acid or HCl as by-products, which is undesirable from both an environmental and economic point of view. Unlike these, the use of carboxylic acids as acylating agents should be ideal, forming ketone, and giving out water as the only by-product [14]. Therefore, herein we performed a representative F−C acylation using octanoic acid and anisole (1).

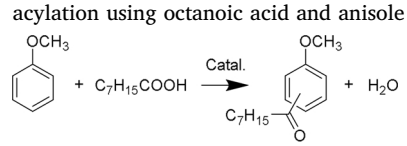

(1)

In addition, by replacing a homogeneous catalyst like aluminum chloride with a heterogeneous catalyst, it was possible to reuse the catalyst and realize an environmentally friendly reaction system. The F-C acylation have been achieved by sulfonic acid functionalized on mesoporous materials [15]. Another synthetic route to obtain aromatic ketones is through the heterogeneous photocatalytic oxidation of

* Corresponding author.
E-mail address: okmr@cc.kogakuin.ac.jp (K. Okumura).

https://doi.org/10.1016/j.mcat.2019.110410
Received 25 March 2019; Received in revised form 14 May 2019; Accepted 17 May 2019

Table 1
Physical properties and Friedel-Crafts acylation of anisole with octanoic acid catalyzed by WO_3 loaded on various kinds of supports.[a]

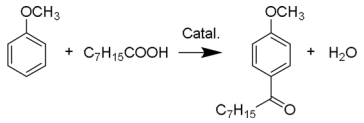

Entry	Support	WO_3 loading / wt%	Acid amount / mol kg^{-1}[b]	BET surface area before the loading of WO_3 / $m^2 g^{-1}$	BET surface area after the loading of WO_3 / $m^2 g^{-1}$	Yield / %[c]
1	MgO	5	0.36	311	202	0
2	Al_2O_3	23	0.26	175	57	7
3	TiO_2 (rutile)	9	0.18	50	34	80
4	TiO_2 (anatase)	18	0.48	105	59	86
5	ZrO_2	17	0.26	120	79	19
6	CeO_2	19	0.18	175	77	0

[a] The amount of WO_3 charged was adjusted to be 4.5 nm^{-2} at the time of preparation. The reaction was performed using 10 g of anisole and 2 mmol of octanoic acid in an oil bath at 413 K for 6 h. The mole ratio of anisole and octanoic acid was 46.2. The amount of catalyst used for reaction was adjusted so that the WO_3 content was 0.018 g.
[b] Measured with NH_3 TPD.
[c] Calculated based on the octanoic acid (2 mmol) used for reaction.

aromatic alcohols [16]. In this study, we compared the catalytic activity of WO_3 supported on various kinds of supports, for F-C reactions. Furthermore, the catalytic performance of WO_3 supported on TiO_2, which exhibited the highest activity, was examined in detail, and the origin of the enhanced catalytic activity of WO_3/TiO_2 in the F-C reaction is discussed.

2. Experimental

2.1. Sample preparation

The supported WO_3 catalyst was prepared by the conventional impregnation method. Typically, a solution of ammonium paratungstate, $(NH_4)_{10}H_2W_{12}O_{42}{\cdot}4H_2O$ (supplied by Wako Pure Chemical Industries, Ltd.) dissolved in 60 ml of water was immersed in the oxide support. The oxides used as support for WO_3 and their physical properties are listed in Tables 1 and 2. MgO (MGO-4), Al_2O_3 (ALO-7), TiO_2 (TIO-4, -16), and CeO_2 (CEO-2) were obtained from the Catalysis Society of Japan. Physical properties (acid amount and surface area) of these supports for WO_3-loaded catalysts are also included in Tables 1 and 2. Unless otherwise stated, the anatase-type (TIO-16; Tables 1 and 2, entry 4) TiO_2 was used as the support for TiO_2. Zeolite-β(HSZ-920HOA) and ZrO_2 (RC-100) were supplied by Tosoh Co. and Daiichi Kigenso Kagaku Kogyo Co., respectively. The ammonium paratungstate solution was evaporated on a water bath with continuous stirring in the presence of the oxide supports. The resulting powder was heat treated in a furnace in air at 773 K for 2 h. The color of the WO_3/TiO_2 samples, calcined in air, changed from white to yellow as the amount of tungsten oxide increased. The amount of WO_3 charged was adjusted to be 4.5 nm^{-2} at the time of preparation, unless otherwise stated (Table 1). This corresponds to the stipulated amount to ensure a monolayer of WO_3 according to the reported cross section of W on Al_2O_3 (0.22–0.245 nm^2/W). [17]. In addition, samples in which the loading amount of tungsten oxide fixed be to 18% by weight were also prepared (Table 2). In the case where TiO_2 was used as a support, the loading of WO_3 was varied in the range from 7 to 100 wt% (pure WO_3).

Table 2
Physical properties and Friedel-Crafts acylation of anisole with octanoic acid catalyzed by 18 wt%-WO_3 loaded on various kinds of supports and zeolite β.[a]

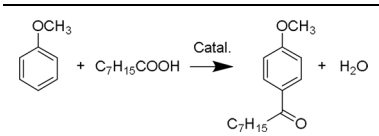

Entry	Support	Acid amount / mol kg^{-1}[b]	BET surface area after the loading of WO_3 / $m^2 g^{-1}$	Yield / %[c]
1	MgO	0.32	149	0
2	Al_2O_3	0.31	118	10
3	TiO_2 (rutile)	0.20	34	48
4	TiO_2 (anatase)	0.48	59	86
5	ZrO_2	0.14	79	34
6	CeO_2	0.13	77	1
7	zeolite β (H-type, Si/Al_2 = 20)[d]	0.58	405	34

[a] The reaction was performed using 10 g of anisole and 2 mmol of octanoic acid with 0.1 g of catalysts in an oil bath at 413 K for 6 h. The mole ratio of anisole and octanoic acid was 46.2.
[b] Measured with NH_3 TPD.
[c] Calculated based on the octanoic acid (2 mmol) used for reaction.
[d] WO_3 is not loaded on zeolite β.

2.2. Characterization

X-ray diffraction (XRD) of the obtained sample was measured using a MiniFlex (Rigaku) X-ray diffractometer (Cu Kα source; 2θ = 10–70°). X-ray photoelectron spectroscopy (XPS) data were collected with an Al anode, using a Quantum 2000 (Ulvac Phi) instrument with a beam diameter of 100 μm and an accelerating voltage of 15 kV. Synchrotron radiation experiments were conducted at BL01B1 with the approval of the Japan Synchrotron Radiation Laboratory (JASRI, Proposal number: 2013B1067). A Si (111) single crystal was used to obtain a monochromatic X-ray beam. Measurements were made in quick mode. In order to collect W L_1- and L_3-edge X-ray absorption fine structure (XAFS) data, ionization chambers filled with N_2 and N_2 (50%)/Ar (50%) were used as I_0 and I, respectively. Data were analyzed using the REX 2000 program (Rigaku). For analysis of W L_3-edge extended X-ray absorption fine structure (EXAFS), Fourier transform of the $k^3\chi$ (k) data was performed in the k range from 25 to 150 nm^{-1}.

The acid properties of the prepared WO_3/TiO_2 catalyst were measured by studying the temperature-programmed desorption (TPD) of ammonia using BelCatII (Microtrac Bel Co.). Prior to measurement, the sample was evacuated at 773 K under He flow. Ammonia (13.3 kPa), diluted with He, was equilibrated with the pretreated sample at 373 K. TPD data was collected at a temperature ramp rate of 10 K/min. A thermal conductivity detector was used for the quantitative determination of desorbed NH_3 from WO_3/TiO_2. N_2 adsorption isotherms were recorded using a BELSORP-mini (Microtrac BEL Co.) instrument.

Fourier-transform infrared (FTIR) spectra were recorded with a resolution of 1 cm^{-1} using a Spectrum One spectrometer (PerkinElmer Co.). Before pyridine was adsorbed, the sample was heat treated at 773 K in air. The treated sample was immersed in a toluene solution of pyridine (Wako co.) at room temperature and subsequently rinsed with hexane. The dried samples were diluted with potassium bromide and pelleted for determination of FTIR.

2.3. F-C acylation

F-C acylation of anisole, with octanoic acid as acylating agent, was carried out using 10 g anisole and 2 mmol octanoic acid in an oil bath at 413 K with Ar bubbling (30 mL/min), unless otherwise stated. The reagents were obtained from Tokyo Chemical Industry Co. When the temperature of the solution reached 413 K, the catalyst was charged to the flask. For recycling, spent catalyst was separated by filtration followed by washing with toluene. After drying at 343 K, the remaining solid was heat-treated in a furnace in 773 K air to remove adsorbed species before recycling. The product was analyzed using a gas chromatograph (GC-2010, Shimadzu) equipped with a capillary column (InertCap1, GL-Science Co.) and a Flame Ionization detector (FID). In the analysis, tridecane was used as an internal standard. Formation of 4-methoxyoctanophenone was confirmed by ^{1}H NMR (Fig. S1). The 1H NMR spectra were recorded on a JEOL JNM-ECZ400S spectrometer (JEOL, Tokyo, Japan) in $CDCl_3$. Upon completion of the reaction, the solvent was removed in vacuo and the crude product was purified by column chromatography on silica gel using hexane and ethyl acetate (9:1) to give 4-methoxyoctanophenone. The F-C reaction using hexanoic acid, heptanoic acid, and decanoic acid (Tokyo Chemical Industry co.) was carried out in the same manner as the reaction using octanoic acid. The resulting mixture was heated at 413 K in N_2 atmosphere and monitored by thin-layer chromatography (TLC) and GC.

3. Results and discussion

3.1. XRD patterns and W L_1- and L_3-edge XAFS

Fig. 1(a) shows the X-ray diffraction (XRD) patterns of supported WO_3/metal-oxides in comparison with those of pure WO_3 crystals and bare metal oxide supports. No diffraction assignable to crystalline WO_3 was observed on CeO_2 and ZrO_2, suggesting that WO_3 is well-dispersed over the entire surface of these oxides. For WO_3/Al_2O_3 and WO_3/TiO_2, a small diffraction assignable to monoclinic WO_3 appeared in the range 23–24° [18]. This suggests that slightly aggregated WO_3 is formed on the surface of Al_2O_3 and TiO_2. Fig. 1(b) focusses on XRD patterns of WO_3/TiO_2, for different addition amounts of WO_3. The diffraction of WO_3/TiO_2 at a WO_3 loading amount of less than 14% by weight is in good agreement with that of anatase TiO_2. On increasing the loading amount to more than 18% by weight, the peak attributable to the monoclinic WO_3 appears, most likely due to the beginning of WO_3 aggregation. As shown in Fig. 1(b), the small peak assignable to the (100) plane of hexagonal WO_3 is also observed in the 78 wt%-WO_3 loaded TiO_2.

W L_1- and L_3-edge XAFS have been frequently used to provide information on local symmetry, coordination, and valency of W oxides supported on metal oxides [19]. Fig. 2 shows radial distribution functions (Fourier-transformed) of WO_3/TiO_2 for different loadings of WO_3, heat treated at 773 K. The corresponding $k^3\chi(k)$ data are displayed in Fig. S2. The peak appearing at 0.14 nm in FT of each sample in Fig. 2 could be attributed to the W—O bond (phase shift uncorrected) straightaway. The peak that appears between 0.24 and 0.30 nm in WO_3/TiO_2, with WO_3 loading of less than 18 wt%, may be assignable to the mixture of W-O-Ti and W—O—W bonds, suggesting a strong interaction between WO_3 and TiO_2 [20,21]. The EXAFS of WO_3/TiO_2 with WO_3 loading higher than 37 wt% was close to that of WO_3 due to the formation of crystalline monoclinic WO_3, as confirmed by the XRD

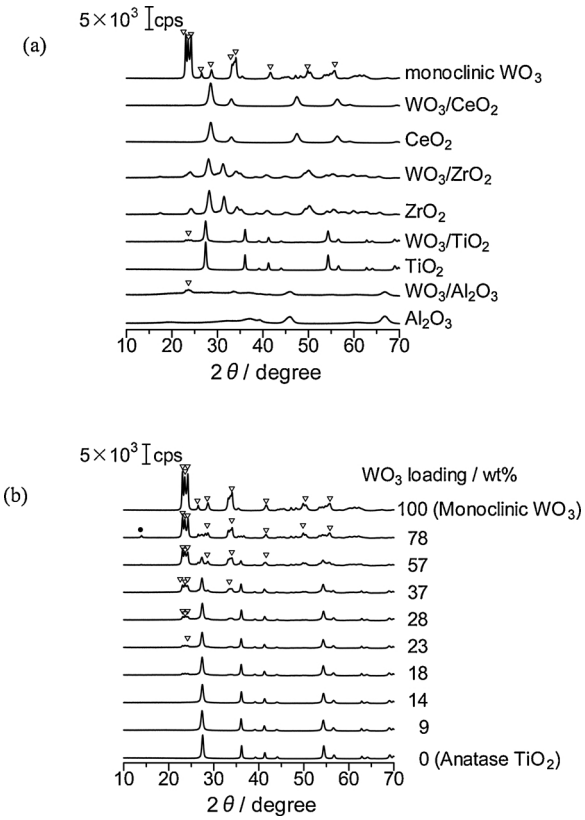

Fig. 1. XRD patterns of (a) WO_3 loaded on various supports, as mentioned in Table 1, and (b) WO_3/TiO_2 with different loadings of WO_3. ▽ and • indicate the diffraction due to the monoclinic and hexagonal phases of the WO_3 crystal, respectively.

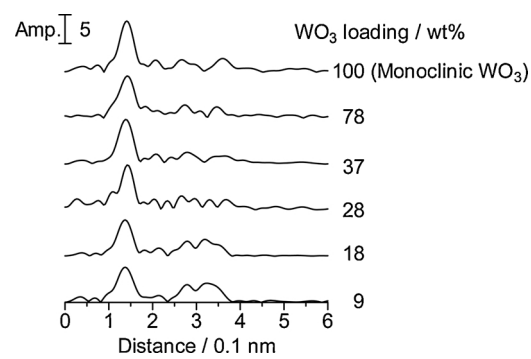

Fig. 2. W L_3-edge EXAFS radial distribution functions of WO_3 loaded on TiO_2 for different loadings of WO_3.

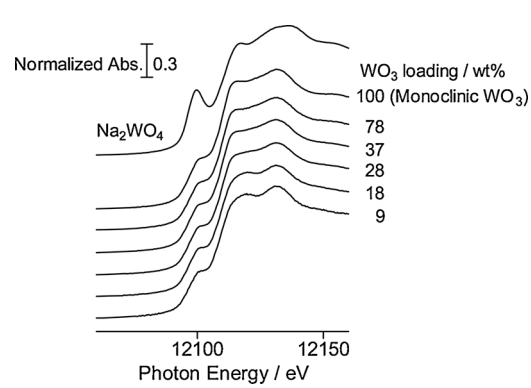

Fig. 3. W-L_1-edge XANES of Na_2WO_4, monoclinic WO_3 and WO_3/TiO_2 for different loadings of WO_3.

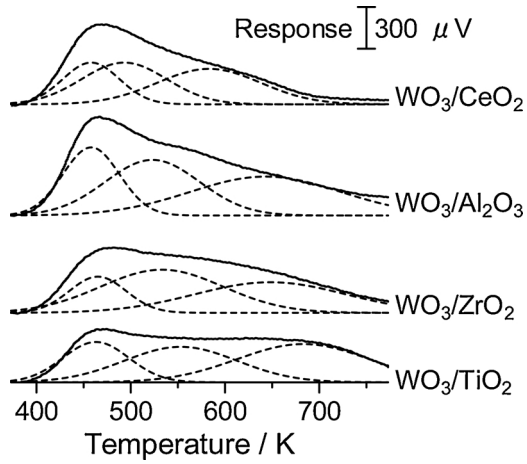

Fig. 4. Raw (solid lines) and simulated (dotted lines) NH_3-TPD curves of WO_3 loaded on different kinds of supports WO_3 loaded on various supports, as mentioned in Table 1.

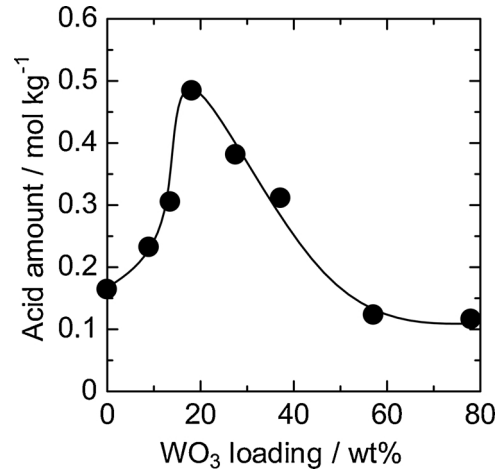

Fig. 5. The dependence of the acid content of WO_3/TiO_2 on the loading of WO_3 on TiO_2 measured with NH_3-TPD.

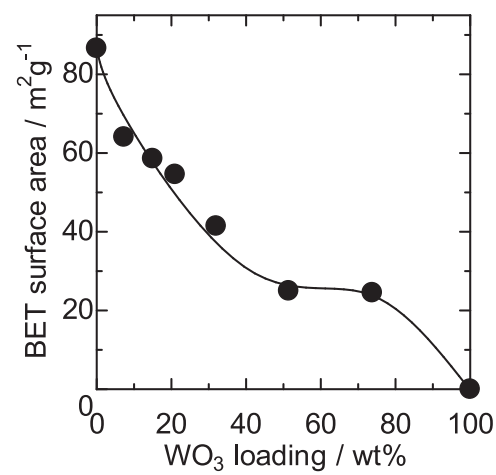

Fig. 6. BET surface area plotted as a function WO_3 loading in WO_3/TiO_2.

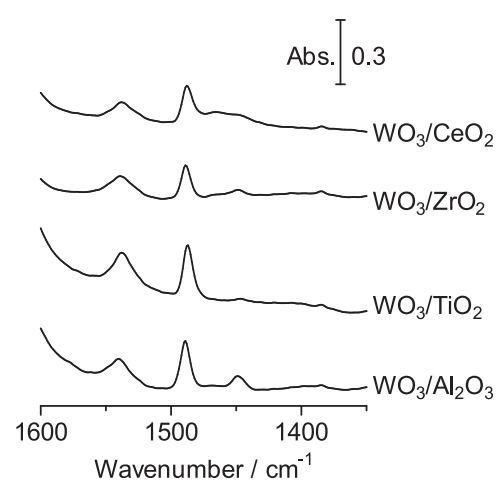

Fig. 7. FTIR spectra of pyridine adsorbed on WO_3 loaded on different kinds of supports, as mentioned in Table 1.

data. The shape of X-ray absorption near edge structure (XANES) did not change relative to the loading amount of WO_3 (Fig. 3). The intensity of the pre-edge peak appearing at 12,100 eV in W L_1-edge XANES remains the same for different loading amounts. The shape is closer to that of monoclinic WO_3, while the intensity of the pre-edge peak is much smaller than that of Na_2WO_4 with tetrahedral symmetry, suggesting that the local symmetry around W is a distorted octahedron [22].

3.2. NH_3-TPD and N_2 adsorption isotherms

Fig. 4 shows the NH_3-TPD curves for WO_3 loaded on different supports corresponding to the samples listed in Table 1. The broad peaks appear in the temperature range between 400 and 800 K, which could be deconvoluted into three peaks, as shown by the dotted lines in the figure. The peak at around 470 K may be attributed to weakly adsorbed NH_3 [23], but the broad peak that appears at higher temperature arises from NH_3 adsorbed at the acidic site of WO_3. The broad peaks shifted depending on the support used. The suggested order of acid strength is as follows: $WO_3/CeO_2 < WO_3/Al_2O_3 < WO_3/ZrO_2 < WO_3/TiO_2$. The amount of acid was measured based on desorption of NH_3 at temperature higher than 470 K, corresponding to where the peak appears. The values, listed in Table 1, will be utilized for calculation of TOF, as will be mentioned later.

Next, NH_3-TPD of WO_3/TiO_2 was measured for samples having different loading amounts of WO_3 (Fig. S3), and the amount of acid measured by the TPD curve was measured as a function of the loading of WO_3 on TiO_2 (Fig. 5). A steep increase in the acid amount is observed for WO_3 loading of less than 14 wt%, probably owing to the even spreading of WO_3 on the surface of TiO_2. When the loading amount of WO_3 is further increased, the acidic part gradually decreases. The highest acid content was obtained with 18 wt% (0.48 mol kg^{-1}). This agrees with the trend published in the literature that the highest acid amount is obtained in the vicinity of the upper layer of WO_3 supported on ZrO_2 [24]. The decrease in acid content may be caused by the aggregation of WO_3, as confirmed by XRD (Fig. 1(b)), resulting in the decrease in surface area.

Fig. S4 shows the N_2 adsorption isotherms, classified as type II, for unloaded TiO_2 and 18 wt% WO_3/TiO_2. Brunauer-Emmet-Teller (BET) surface area was calculated based on the isotherms. The BET surface area gradually decreased from 88 to 25 $m^2 g^{-1}$ with an increase in the amount of the added WO_3 from 0 (TiO_2) to 78 wt% (Fig. 6). This trend may be due to the formation of aggregated WO_3, as confirmed by XRD.

3.3. FTIR Spectra of adsorbed pyridine

Fig. 7 shows the IR spectrum of pyridine adsorbed on WO_3 supported on the selected supports. The broadband for pyridine species adsorbed at the Brønsted acid site typically appears at 1530 cm^{-1}, while that for the corresponding Lewis acid site should appear at ca.

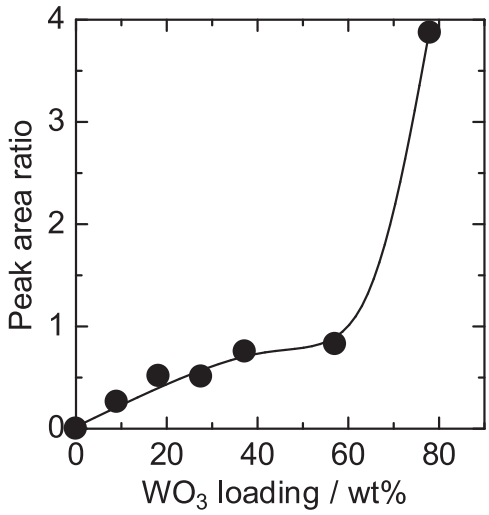

Fig. 8. The relationship between the loading of WO_3 and the ratio of the W-4d and Ti-2p peak areas of WO_3/TiO_2 determined by XPS.

1450 cm^{-1}. The intense peak observed at 1530 cm^{-1} for the employed samples, while the missing peak at 1450 cm^{-1}, regardless of the catalyst used, except for WO_3/Al_2O_3, shows that Brønsted acid sites were predominant in WO_3-loaded samples. FTIR spectra of pyridine adsorbed on WO_3/TiO_2 for different loadings of WO_3 are shown in Fig. S5. Brønsted acid sites were predominant here as well, regardless of the loading amounts of WO_3. The peak assigned to adsorbed pyridine did not appear on bare TiO_2, suggesting that the Brønsted acid site was generated only after the addition of WO_3.

3.4. XPS

To obtain information on the valence state of W exposed to the surface, XPS was measured using a sample loaded with WO_3. The photoelectron energy of the peak appearing in XPS of W 4d showed that the valence of W was 6 +, regardless of the type of support (Fig. S6(a)). On the other hand, in the case of WO_3/TiO_2, with an increase in the amount of WO_3, the binding energy of Ti 2p peaks shifts to a higher value (Fig. S6(b)). This could be because of the slight change in the electronic state of Ti after the addition of WO_3, although the reason was not clearly understood at this stage. Fig. 8 shows the peak area ratio of W 4d and Ti 2p plotted as a function of the amount of WO_3 added. This ratio increased almost linearly as the content of WO_3 increased to 57% by weight. Unlike the previous report regarding the relationship between the peak area of Raman spectra and the surface density of W in WO_3/ZrO_2 [25], no clear reflection point was observed in the case of WO_3/TiO_2, suggesting that the obvious transformation from 2D to 3D did not take place, even after the generation of WO_3 clusters with low loading of WO_3. When the loading of WO_3 reached 78% by weight, a sharp increase in the ratio was observed, probably due to the onset of vigorous aggregation of WO_3. This fact agrees with the appearance of diffraction assignable to the aggregated WO_3 in the XRD pattern of the samples with a larger loading amount than 78 wt% (Fig. 1(b)).

3.5. F-C acylation

Regardless of the WO_3 supported catalyst used in the reaction between octanoic acid and anisole, para-substituted ketones were obtained with a selectivity higher than 97%, with small amounts of methyl octanoate and phenyl octanoate as byproducts. The reaction proceeded similar to that on a self-assembly of Nb-W nanofibers [26]. The reaction was performed with the use of different mol ratios of anisole and octanoic acid over WO_3/TiO_2. The yield decreased monotonically accompanied by decrease in the molar ratio (Fig. S7). Table 1 reports the % yield of the F-C alkylation for WO_3 loaded on different types of supports in which the amount of catalyst used for reaction was adjusted so that the WO_3 content was 0.018 g. The amount of WO_3 charged in Table 1 was adjusted to be 4.5 nm^{-2} at the time of preparation. A particularly high yield was obtained when TiO_2 was used as a support. A similar tendency was observed in the catalytic performance of the 18 wt%-WO_3 loaded samples (Table 2). In the case of WO_3/MgO, the reaction solution became viscous. Analysis by GC revealed that octanoic acid was completely consumed after the reaction even though 4-methoxyoctanophenone was not detected in the solution. Probably octanoic acid reacted with MgO to produce magnesium caprylate. The yield (86%; Table 1 and 2, entry 4) of WO_3/TiO_2 was much higher than that obtained with zeolite β (32%; Table 2, entry 7), which has been recognized as a promising catalyst for the reaction [27,28]. There was no appearance of an induction period in the reaction using WO_3/TiO_2 (Fig. S8). The yield of product obtained at 6 h with WO_3 loaded on TIO-16 with anatase structure (86%) was close to that of WO_3 on TIO-4 with rutile structure (80%, Table 1, entry 3). It can be concluded that the crystal structure of the support had little influence on the support structure, which can also be confirmed from the fact that the curves for yield vs. time of reaction overlap (Fig. S8). The yield of 4-methoxyoctanophenone for WO_3/ZrO_2 was much lower than that of WO_3/TiO_2 (Table 1, entry 5). Since the catalyst has been reported to be active in the acylation of acetic acid with toluene, this seems rather unexpected [29].

The yield of 4-methoxyoctanophenone, measured with GC, plotted as a function of the amount of WO_3 loaded onto the TiO_2 support is shown in Fig. 9. Data was collected at 2 h and 6 h after the start of the reaction. A sharp increase in yield was observed for an increase in the loading amount from 0 to 20 wt% of WO_3. On further increasing the loading, the yield gradually decreased. The highest yield (90%) was obtained at ca. 20% by weight. On plotting the yield at 2 h as a function of the amount of WO_3, the highest value was obtained for 26 wt%. This is slightly higher than the value corresponding to the upper layer coverage of WO_3 (18 wt%), and diffraction attributable to crystalline WO_3 was clearly observed in XRD (Fig. 1(b)) for loadings above 18 wt %. Slightly crystallized WO_3 is therefore suggested as a catalyst for the F-C reaction.

To study the recyclability of the catalyst, the spent catalyst was collected by filtration and subsequently rinsed with toluene. The obtained solid was then heat-treated in air at 773 K for 3 h to remove carbonaceous deposits. No deactivation was observed even when used at least 5 times, as shown in Fig. 10.

Catalytic reactions using anisole and carboxylic acids with different

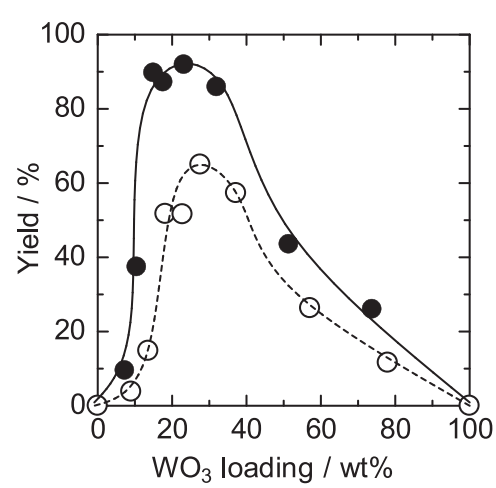

Fig. 9. Yield of 4-methoxyoctanophenone plotted as a function of WO_3 loading on TiO_2. Reaction time: 2 h (○) and 6 h (•). The yield was calculated based on the quantity of octanoic acid (2 mmol) used for reaction.

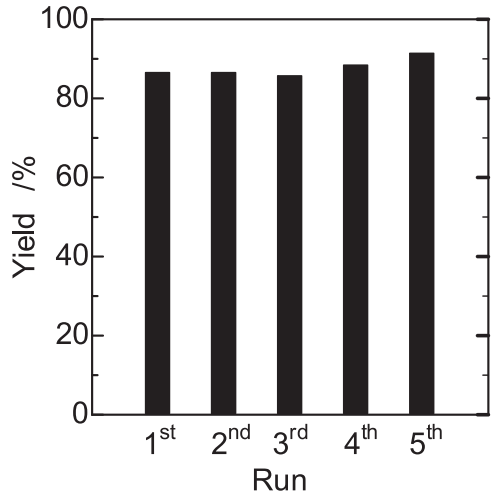

Fig. 10. Yield of 4-methoxyoctanophenone in the repeated reaction between octanoic acid and anisole over 18 wt%-WO_3/TiO_2. Reaction time: 6 h. For recycle use, the catalyst was washed with toluene, dried and calcined in air at 773 K.

Table 3
Friedel-Crafts acylation of anisole with carboxylic acids with different linear alkyl chain lengths catalyzed by 18 wt%-WO_3/TiO_2.[a]

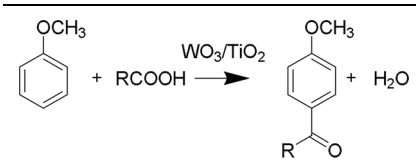

R	Yield / %[b] (anisole / acid = 46.2[c])	Yield / %[b] (anisole / acid = 10.0[c])
C_5H_{11}	84	63
C_6H_{13}	91	72
C_7H_{15}	86	67
C_9H_{19}	95	62

[a] The reaction was performed under the same condition given in the footnote of Table 2.
[b] Calculated based on the octanoic acid (2 mmol) used for reaction.
[c] Molar ratio of anisole and octanoic acid.

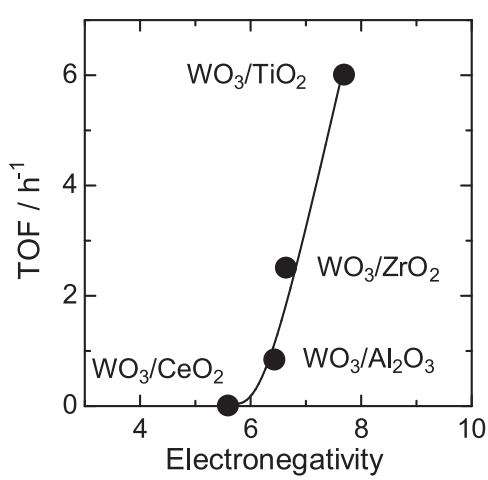

Fig. 11. TOF in the F-C reaction over WO_3 loaded on various supports as mentioned in Table 1 plotted as a function of the electronegativity of support cation.

linear alkyl chain lengths were carried out at 18 wt% WO_3/TiO_2 to explore the scope of the catalyst. We see that the yield is not dependent on the chain length of the carboxylic acid, which indicates the generality of the application of the WO_3/TiO_2 catalyst (Table 3).

3.6. Proposed mechanism for the high catalytic activity of WO_3/TiO_2

Based on the data on catalyst performance and NH_3-TPD, the TOF was plotted as a function of the electronegativity of the cation of the corresponding oxide support (Fig. 11). For the calculation of TOF, the molar amount of the product (4-methoxyoctanophenone) was divided by the desorption amount (mol) of NH_3 measured by NH_3-TPD. Electronegativity was recognized as being indicative of acid or base properties of metal oxides. Values for metal cations are expressed in Pauling and were derived from the corresponding values for the elements using eq. 2 [30]:

$$x_i = (1 + 2i)\, x_0 \quad (2)$$

Here, i and x_0 indicate the valence and electronegativity of the element, respectively [9,31]. In other words, the smaller the electronegativity of oxides, the higher the basicity, and vice versa. Accordingly, the NH_3-TPD peak shifted to a higher temperature with an increase in x_i. TOF showed a sharp increase with increasing electronegativity of the support, as given in Fig. 11. As a result, WO_3/TiO_2 exhibited the highest TOF. It is proposed that the low activity of WO_3/CeO_2 was caused by the neutralization or weakening of the acidic sites of WO_3, due to the electron donating effect of CeO_2, which had the highest basicity among the employed supports. In contrast, because the base strength of TiO_2 is the weakest, it resulted in the highest activity of WO_3/TiO_2 among the catalysts used, so that the inherent acid properties of WO_3 were retained to a greater extent on a TiO_2 support. According to the density functional theory calculations in the literature, protons prefer the bridging oxygen sites of corner-sharing WO_6, suggesting that these protons acted the active sites for F-C reaction [32].

4. Conclusions

We have found that the catalytic activity of WO_3 in the F-C acylation with octanoic acid and anisole varies depending on the support used. The highest activity was obtained when TiO_2 was used as a support. The catalyst was also applicable for similar reactions involving carboxylic acids other than octanoic acid. TOF was found to be dependent on the electronegativity of the cation of the support, implying that the electron withdrawing or donating effect of the support determines the Brønsted acid strength and catalytic activity of the supported WO_3. We believe that such a general understanding of the acid-base interaction between the support and the supported oxide provides new insight into the origin of the catalytic activity of the supported metal oxide catalyst.

Acknowledgements

This research was supported by the Ministry of Education, Science, Sports and Culture, Grant-in-Aid for Scientific Research (C), 16K06859, 2016–2018.

Appendix A. Supplementary data

Supplementary material related to this article can be found, in the online version, at doi:https://doi.org/10.1016/j.mcat.2019.110410.

References

[1] H. Zheng, J.Z. Ou, M.S. Strano, R.B. Kaner, A. Mitchell, K. Kalantar-zadeh, Adv. Funct. Mater. 21 (2011) 2175–2196.
[2] J. Polleux, A. Gurlo, N. Barsan, U. Weimar, M. Antonietti, M. Niederberger, Angew. Chem. 118 (2006) 267–271.

[3] K. Okumura, S. Ishida, T. Tomiyama, M. Niwa, Chem. Lett. 40 (2011) 527–529.
[4] K. Okumura, T. Tomiyama, S. Shirakawa, S. Ishida, T. Sanada, M. Arao, M. Niwa, J. Mater. Chem. 21 (2011) 229–235.
[5] B. Gao, Y. Ma, Y. Cao, W. Yang, J. Yao, J. Phys. Chem. B 110 (2006) 14391–14397.
[6] V. Logie, G. Maire, D. Michel, J.-L. Vignes, J. Catal. 188 (1999) 90–101.
[7] C.D. Baertsch, K.T. Komala, Y.-H. Chua, E. Iglesia, J. Catal. 205 (2002) 44–57.
[8] C. Yue, G. Li, E.A. Pidko, J.J. Wiesfeld, M. Rigutto, E.J.M. Hensen, ChemSusChem 9 (2016) 2421–2429.
[9] K. Okumura, T. Kobayashi, H. Tanaka, M. Niwa, Appl. Catal. B Environ. 44 (2003) 325–331.
[10] T. Kim, A. Burrows, C.J. Kiely, I.E. Wachs, J. Catal. 246 (2007) 370–381.
[11] D.G. Barton, M. Shtein, R.D. Wilson, S.L. Soled, E. Iglesia, J. Phys. Chem. B 103 (1999) 630–640.
[12] T. Kitano, T. Hayashi, T. Uesaka, T. Shishido, K. Teramura, T. Tanaka, ChemCatChem 6 (2014) 2011–2020.
[13] G. Sartori, R. Maggi, Chem. Rev. 106 (2006) 1077–1104.
[14] M. Kawamura, D.-M. Cui, S. Shimada, Tetrahedron 62 (2006) 9201–9209.
[15] E. Doustkhah, J. Lin, S. Rostamnia, C. Len, R. Luque, X. Luo, Y. Bando, K.C.-W. Wu, J. Kim, Y. Yamauchi, Y. Ide, Chem. Eur. J. 25 (2019) 1614–1635.
[16] J.C. Colmenares, R. Luque, Chem. Soc. Rev. 43 (2014) 765–778.
[17] C. Pfaff, M.J. Pérez Zurita, C. Scott, P. Patiño, M.R. Goldwasser, J. Goldwasser, F.M. Mulcahy, M. Houalla, D.M. Hercules, Catal. Lett. 49 (1997) 13–16.
[18] J. Zhu, S. Wang, S. Xie, H. Li, Chem. Commun. (Camb.) 47 (2011) 4403–4405.
[19] M. Fernández-García, A. Martínez-Arias, A. Fuerte, J.C. Conesa, J. Phys. Chem. B 109 (2005) 6075–6083.
[20] A. Burrows, C.J. Kiely, R.W. Joyner, H.K. Knözinger, F. Lange, Catal. Lett. 39 (1996) 219–231.
[21] S. Yamazoe, Y. Hitomi, T. Shishido, T. Tanaka, J. Phys. Chem. C 112 (2008) 6869–6879.
[22] J.A. Horsley, I.E. Wachs, M. Brown, G.H. Via, F.D. Hardcastle, J. Phys. Chem. 91 (1987) 4014–4020.
[23] T. Miyamoto, N. Katada, J.-H. Kim, M. Niwa, J. Phys. Chem. B 102 (2002) 6738–6745.
[24] N. Naito, N. Katada, M. Niwa, J. Phys, Chem. B 103 (1999) 7206–7213.
[25] W. Zhou, N. Soultanidis, H. Xu, M.S. Wong, M. Neurock, C.J. Kiely, I.E. Wachs, ACS Catal. 7 (2017) 2181–2198.
[26] K. Okumura, S. Ishida, R. Takahata, N. Katada, Catal. Today 204 (2013) 197–203.
[27] M.L. Kantam, K.V.S. Ranganath, M. Sateesh, K.B.S. Kumar, B.M. Choudary, J, . Mol. Catal. A Chem. 225 (2005) 15–20.
[28] U. Freese, F. Heinrich, F. Roessner, Catal. Today 49 (1999) 237–244.
[29] K. Arata, H. Nakamura, M. Shouji, Appl. Catal. A Gen. 197 (2000) 213–219.
[30] L. Pauling, J. Am. Chem. Soc. 54 (1932) 3570.
[31] K. Tanaka, M. Ozaki, K. Tamaru, Shokubai 6 (1964) 262–265.
[32] H. Lin, F. Zhou, C.P. Liu, V. Ozoliņš, J. Mater. Chem. A Mater. Energy Sustain. 2 (2014) 12280–12288.